Chinese Chemical Letters 32 (2021) 2279–2282

Contents lists available at ScienceDirect

Chinese Chemical Letters

journal homepage: www.elsevier.com/locate/cclet

Communication

A co-activation strategy for enhancing the performance of hematite in photoelectrochemical water oxidation

Boyao Xie[a,b,1], Xingming Ning[a,1], Shuoming Wei[a], Jia Liu[a], Jimei Zhang[b,*], Xiaoquan Lu[a,*]

[a] Tianjin Key Laboratory of Molecular Optoelectronic Science, Department of Chemistry, School of Science, Tianjin University, Tianjin 300072, China
[b] State Key Laboratory of Separation Membranes and Membrane Processes, School of Chemistry and Chemical Engineering, Tiangong University, Tianjin 300387, China

ARTICLE INFO

Article history:
Received 6 November 2020
Received in revised form 29 December 2020
Accepted 3 January 2021
Available online 9 January 2021

Keywords:
Photoelectrochemical
Phosphorus doping
Charge separation
CoAl-LDHs
Hematite

ABSTRACT

Hematite (α-Fe_2O_3) is a promising photoanode for photoelectrochemical (PEC) water splitting. However, the severe charge recombination and sluggish water oxidation kinetics extremely limit its use in photo-hydrogen conversion. Herein, a co-activation strategy is proposed, namely through phosphorus (P) doping and the loading of CoAl-layered double hydroxides (CoAl-LDHs) cocatalysts. Unexpectedly, the integrated system, CoAl-LDHs/P-Fe_2O_3 photoanode, exhibits an outstanding photocurrent density of 1.56 mA/cm^2 at 1.23 V (*vs.* reversible hydrogen electrode, RHE), under AM 1.5 G, which is 2.6 times of pure α-Fe_2O_3. Systematic studies reveal that the remarkable PEC performance is attributed to accelerated surface OER kinetics and enhanced carrier separation efficiency. This work provides a feasible strategy to enhance the PEC performance of hematite photoanodes.

With the increasingly serious energy crisis and environmental pollution problems, photoelectrochemical (PEC) water splitting using sunlight to generate hydrogen has been regarded as a feasible way to achieve sustainable development [1]. Early-stage, numerous semiconductor materials, such as ZnO [2], $BiVO_4$ [3], WO_3 [4] and CdS [5] have been widely studied as photoanodes for PEC water splitting. Hematite (α-Fe_2O_3), a stable n-type semiconductor, stands out because of its nontoxicity, earth-abundance, and suitable band gap (2.1 eV) [6]. It absorbs about 40% of solar radiation, and the maximum theoretical photocurrent density can reach 12.6 mA/cm^2 under AM 1.5 G illumination [7].

However, pure hematite photoanode suffers from poor conductivity, short hole diffusion distance ($\approx$ 2 nm) [8], sluggish oxygen evolution kinetics [9], low carrier concentration, and severe recombination problems [10], which result in the PEC water splitting performance that can be achieved at present is still far below the theoretical limit. Various strategies have been proposed to solve these obstacles, including loading oxygen evolution cocatalysts (OECs) [11,12], forming heterojunctions [13,14], nanostructure engineering [15,16] and surface passivation [17].

Element doping, an effective strategy to modify the charge transport properties of photoanodes bulk phase, could distort the crystal lattice, leading to polaron jumping or increasing the carrier concentration and conductivity of the α-Fe_2O_3 photoanodes [18]. Early-stage, metal doping has been widely used in hematite photoanodes, such as Ti^{4+} [19], Sn^{4+} [20], Zr^{4+} [21] and Cd^{2+} [22]. However, it is inevitable to introduce new energy levels between the valence band and the conduction band of hematite during doping, resulting in more severe charge recombination [23]. The introduction of nonmetallic elements into hematite can address the recombination issue of metal ion doping because the energy state caused by nonmetal dopants is generally above the conduction band of hematite [24]. As an electron donor, nonmetallic phosphorus (P) is a promising candidate for hematite doping, which has more valence electrons than many metal doping elements [25]. Moreover, compared with other dopant—O bonds, the P—O bond in hematite possesses a more covalent nature, which can effectively avoid the formation of deep electron capture sites in hematite [26].

The issue of charge separation in the bulk of hematite is solved by non-metallic doping. However, the sluggish surface reaction kinetics is still an important reason that limits the performance of α-Fe_2O_3 photoanode in PEC water oxidation. Compared with the generation speed of carriers in hematite, surface reactions commonly take place in a longer time range [27]. Up to now, it has been extensively studied by loading cocatalysts on its surface,

* Corresponding authors.
E-mail addresses: zhangjimei6d311@163.com (J. Zhang), luxq@tju.edu.cn (X. Lu)

[1] These authors contributed equally to this work.

https://doi.org/10.1016/j.cclet.2021.01.003
1001-8417/

which can reduce the overpotential and accelerate the reaction kinetics of the hematite surface, including Co-Pi [28], IrO_x [29], NiOOH [30], Co_3O_4 [31], layered double hydroxides (LDHs) [32], *etc*. LDHs stand out because of their low cost, feasible moderation of interlayer object, and excellent stability, which have been regarded to be a promising OECs for PEC water oxidation [33–36].

Herein, we propose a co-activation strategy to solve the charge recombination and sluggish surface reaction of α-Fe_2O_3 through P doping and the loading of CoAl-LDHs OECs. The resulting CoAl-LDHs/P-Fe_2O_3 photoanodes shows an outstanding water oxidation photocurrent density of 1.56 mA/cm^2 at 1.23 V (*vs*. RHE) under AM 1.5 G (100 mW/cm^2) illumination, which is 2.6 times of pure α-Fe_2O_3. Besides, the onset potential is negatively shifted to 0.7 V (*vs*. RHE) and the surface charge separation efficiency is increased to 68.8% at 1.23 V (*vs*. RHE). Our research provides a feasible strategy to enhance the PEC performance of α-Fe_2O_3 photoanodes.

The α-Fe_2O_3 photoanodes were fabricated by a previously reported hydrothermal approach followed by annealing [37]. As shown in Fig. 1a, the α-Fe_2O_3 photoanodes show a nanorods structure on the fluorine-doped SnO_2 (FTO) substrates, which is consistent with the transmission electron microscope (TEM) image (Fig. 2a). The high-resolution transmission electron microscope (HRTEM) image of α-Fe_2O_3 photoanodes (Fig. 2b) shows that the interval of the adjacent lattice plane is 0.25 nm, which is matched with the (110) plane of hematite. The crystallization of different photoanodes were investigated by X-ray diffraction (XRD) patterns (Fig. S2a in Supporting information). The diffraction peaks of α-Fe_2O_3 photoanodes at 36.1° and 64.4° are indexed as the (110) and (300) crystal plane of hematite (JCPDS card number 33-0664), respectively. Besides, the diffraction peak intensity of (110) crystal plane is higher than that of (300) crystal plane, indicating that the (110) crystal plane is mainly exposed in the α-Fe_2O_3 photoanodes, which is more conducive to the transfer of photogenerated charges [38]. As indicated by X-ray photoelectron spectroscopy (XPS), the binding energies of Fe $2p_{1/2}$ and Fe $2p_{3/2}$ for α-Fe_2O_3 are 723.5 eV and 709.6 eV respectively (Fig. S3a in Supporting information), consistent with literature reports [39]. In Fig. S3b (Supporting information), the O 1s spectrum of α-Fe_2O_3 can be decomposed into three peaks. The peak at 529.4 eV is characteristic of the O^{2-} species (designated as Fe-O) in the Fe_2O_3, while the other two peaks are attributed to surface labile oxygen, such as chemisorbed active O, including O_2^{2-} and O^- (531.2 eV, designated as O*) and adsorbed molecular water (532.7 eV, designated as O_w) [40,41]. Scanning electron microscopy (SEM), TEM, HRTEM, XRD and XPS results indicate the successful preparation of the α-Fe_2O_3 photoanodes.

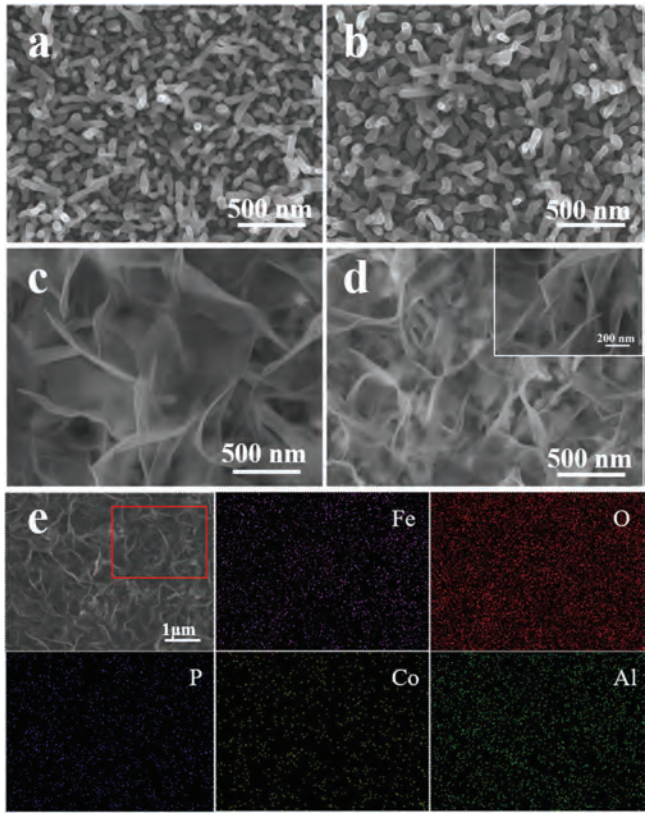

Fig. 1. SEM images of (a) α-Fe_2O_3 NRs photoanodes, (b) P-Fe_2O_3 NRs photoanodes, (c) CoAl-LDHs/Fe_2O_3 photoanodes and (d) CoAl-LDHs/P-Fe_2O_3 photoanodes. (e) SEM-EDX elemental mapping images of Fe, O, P, Co, Al in CoAl-LDHs/P-Fe_2O_3 photoanodes.

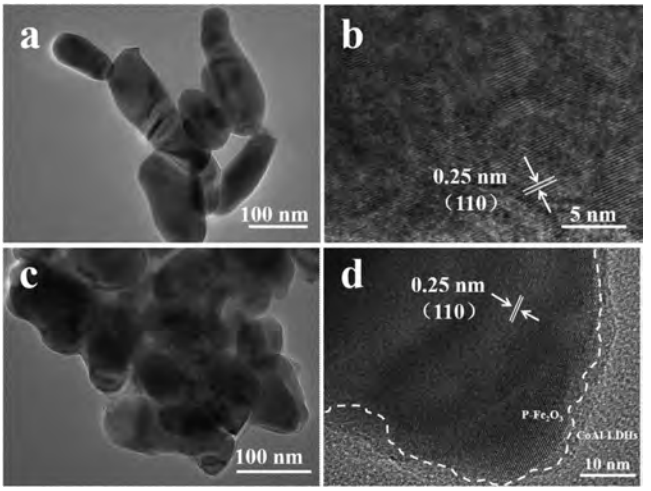

Fig. 2. TEM images of (a) α-Fe_2O_3 NRs photoanodes and (c) CoAl-LDHs/P-Fe_2O_3 photoanodes. HRTEM images of (b) α-Fe_2O_3 NRs photoanodes and (d) CoAl-LDHs/P-Fe_2O_3 photoanodes.

The morphology of P-Fe_2O_3 (Fig. 1b) obtained by the annealing process is unchanged compared to the α-Fe_2O_3 photoanodes. As shown in Fig. S2a, the XRD pattern of the P-Fe_2O_3 photoanodes is the same as the α-Fe_2O_3 photoanodes, which implies that P doping does not affect the crystal structure of α-Fe_2O_3. In Fig. S3a, it is observed that the Fe 2p spectra of P-Fe_2O_3 and CoAl-LDHs/P-Fe_2O_3 are almost the same for the α-Fe_2O_3 photoanodes, indicating that the P doping and the loading of CoAl-LDHs OECs do not affect the chemical states of Fe atoms. As shown in Fig. S3c (Supporting information), it can be obviously seen that the peak at approximately 132.4 eV can be indexed to P^{5+} specie [42]. The Fe 2p and P 2p signals of CoAl-LDHs/P-Fe_2O_3 samples are close to that of $FePO_4$, which indicates a strong interaction between the Fe and P in photoanodes [25]. SEM, XRD and XPS results show that the P-Fe_2O_3 photoanodes were successfully prepared.

As shown in Fig. 1d, when CoAl-LDHs were loaded onto the P-Fe_2O_3 photoanodes, their surface morphology demonstrates a significant change with nanosheets clearly shown on the surface, which is the same as CoAl-LDHs/Fe_2O_3 photoanodes (Fig. 1c). Energy-dispersive X-ray spectrum (EDX) mappings (Fig. 1e) of Fe, O, P, Co and Al illustrate that each element distributes homogeneously in the nano-arrays. The TEM image (Fig. 2c) reveals CoAl-LDHs OECs compactly coated on the surface of α-Fe_2O_3, which would facilitate the separation and transfer of photogenerated carriers in bulk α-Fe_2O_3. The CoAl-LDHs/P-Fe_2O_3 photoanodes displays a lattice spacing of 0.25 nm (Fig. 2d), indicating that the crystal structure of hematite remains unchanged after introducing

phosphorus dopant into the hematite lattice. In Fig. S2a, the XRD pattern of the CoAl-LDHs/P-Fe_2O_3 photoanodes is the same as the α-Fe_2O_3 photoanodes, which implies that P doping and loading of CoAl-LDHs OECs do not affect the crystal structure of α-Fe_2O_3. These analysis results are consistent with HRTEM. The ultraviolet-visible (UV–vis) diffuse reflectance spectra of different photoanodes (Fig. S2b in Supporting information) reveal that P doping and the loading of CoAl-LDHs could only slightly enhance the light absorption ability of α-Fe_2O_3 photoanodes, indicating that the main factors affecting the PEC performance of hematite are charge separation and surface reaction kinetics [43]. As indicated by Fig. S3b, the O* peak becomes strong, which can be ascribed to the OH^- groups in CoAl-LDHs, indicating that the CoAl-LDHs OECs cover the surface of P-Fe_2O_3 photoanodes. The above results show the successful preparation of the CoAl-LDHs/P-Fe_2O_3 photoanodes. The Co 2p core-level spectra are utilized to investigate the valences of Co species in the CoAl-LDHs/P-Fe_2O_3 photoanodes (Fig. S3d in Supporting information). The Co 2p core lines are divided into two peaks of Co $2p_{1/2}$ (797.2 eV) and Co $2p_{3/2}$ (781.3 eV) accompanied by two satellite bands at 803.4 eV and 786.1 eV respectively, indicating that the Co cation exists as high-spin Co^{2+} in CoAl-LDHs/P-Fe_2O_3 photoanodes [44].

The PEC water oxidation activities of different photoanodes were evaluated by measuring the photocurrent–voltage (*J–V*) curves in 1 mol/L NaOH (pH 13.6) under AM 1.5 G simulated sunlight (100 mW/cm^2). From the *J–V* curves in Fig. 3a, we can observe that the pure α-Fe_2O_3 shows a low photocurrent density of 0.6 mA/cm^2 at 1.23 V (*vs.* RHE). When the α-Fe_2O_3 photoanodes are modified with phosphorus doping, the P-Fe_2O_3 photoanodes display a much higher photocurrent density than that of the α-Fe_2O_3 photoanodes due to the carrier density (N_d) of P-Fe_2O_3 photoanodes (1.37×10^{20} cm^{-3}) increased by 2.89 times compared with pure hematite (Fig. 3b). Moreover, CoAl-LDHs/Fe_2O_3 photoanodes demonstrate an enhanced photocurrent density compared to the α-Fe_2O_3 photoanodes, while a pure CoAl-LDHs photoanode in 1 mol/L NaOH electrolyte shows a photocurrent and dark current densities of almost zero at 1.23 V (*vs.* RHE), which indicates that the CoAl-LDHs OECs accelerate the water oxidation kinetics rather than photosensitivity (Fig. S10 in Supporting information). When P doping and loading the CoAl-LDHs cocatalysts for hematite at the same time, the photoanodes exhibit a photocurrent density of 1.56 mA/cm^2 at 1.23 V (*vs.* RHE), which is 1.6 times higher than that of pure α-Fe_2O_3. Besides, the onset potential shows a cathodic shift of 100 mV, indicating a lower overpotential for water oxidation. The maximum applied bias photon-to-current efficiency (ABPE) of the CoAl-LDHs/P-Fe_2O_3 photoanodes achieves 0.20% at 1.0 V (*vs.* RHE), which is 3.84 times that of the bare α-Fe_2O_3 photoanodes (Fig. 3c).

Electrochemical impedance spectroscopy (EIS) measurement was performed to investigate the charge transport properties of the photoanodes under AM 1.5 G illumination (Fig. 3d) [45]. According to the EIS results, the semidiameter of the semicircle of P-Fe_2O_3 and CoAl-LDHs/Fe_2O_3 photoanodes are dramatically reduced compared to pure α-Fe_2O_3, indicating that P doping could reduce the surface charge trapping of hematite, and CoAl-LDHs cocatalysts can effectively facilitate the transport of holes into the electrolyte for water oxidation. Moreover, compared to other photoanodes, the semidiameter of the semicircle of CoAl-LDHs/P-Fe_2O_3 is the smallest, further confirming that the photoanodes have the best charge transport performance, which is consistent with the PEC results.

Photoluminescence (PL) spectra and time-resolved photoluminescence (TRPL) emission decay spectra can be used to evaluate the recombination degree of photo-generated carriers in semiconductors in photocatalysis [3]. A long carrier lifetime and low fluorescence intensity mean efficient charge separation for photoanodes. In Fig. 4a, all samples have the same emission peak at 597 nm, and the fluorescence intensity of α-Fe_2O_3 is the strongest, indicating that pure hematite suffers from severe carrier recombination. In contrast, the fluorescence intensity of P-Fe_2O_3 and CoAl-LDHs/Fe_2O_3 are reduced, and the average fluorescence lifetimes both increase (Fig. 4b), indicating that P doping and the loading of CoAl-LDHs OECs can inhibit the recombination of hematite photo-generated carriers. Among them, the average fluorescence lifetimes of the CoAl-LDHs/P-Fe_2O_3 photoanode is 3.136 ns, 1.25 times higher than that of α-Fe_2O_3, exhibiting the most excellent carrier separation efficiency, which is consistent with the PEC results. This result is further confirmed by the surface charge separation efficiencies of different photoanodes (Fig. 4c). A high surface charge separation efficiency (68.8%) is obtained for CoAl-LDHs/P-Fe_2O_3 photoanodes compared with that of the pure α-Fe_2O_3 (53.7%) at 1.23 V (*vs.* RHE). The stability of the

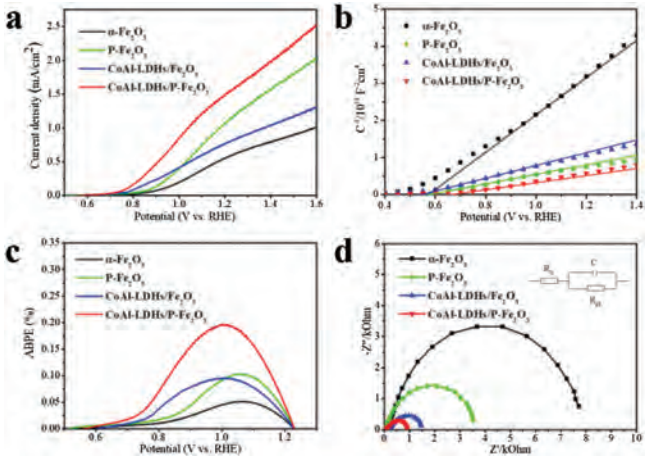

Fig. 3. (a) *J–V* curves of different photoanodes measured with 1 mol/L NaOH (pH 13.6) under AM 1.5 G simulated sunlight (100 mW/cm^2). (b) Mott-Schottky plots of different samples measured in 1 mol/L NaOH solution in dark (1 kHz). (c) ABPE of different photoanodes. (d) EIS Nyquist plots of different photoanodes. The inset reveals equivalent circuit for different photoanodes in the light.

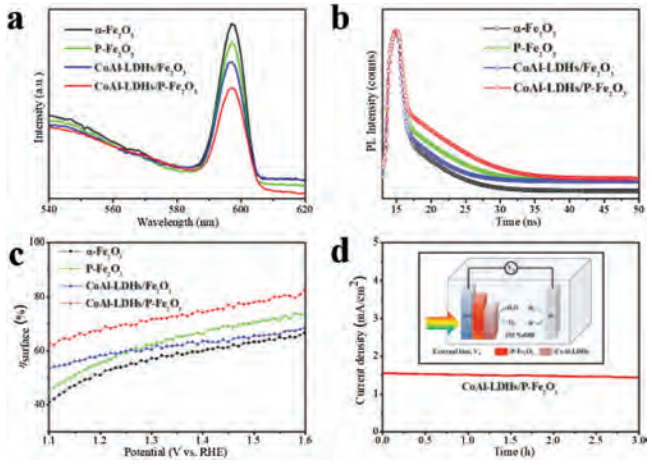

Fig. 4. (a) PL spectra of different samples. (b) TRPL emission decay spectra of different photoanodes. (c) The surface charge separation efficiencies of different photoanodes. (d) *I-t* curves for CoAl-LDHs/P-Fe_2O_3 photoanodes measured at 1.23 V (*vs.* RHE) in 1 M NaOH solution under AM 1.5 G illumination (100 mW/cm^2). The inset shows the schematic of PEC cell for water splitting.

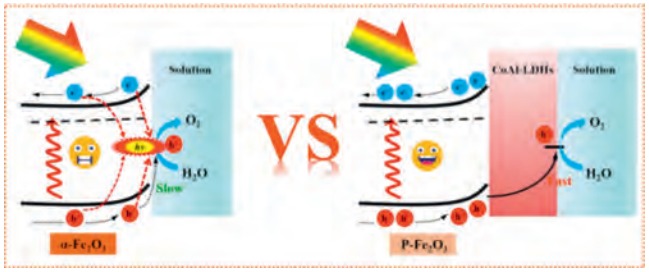

Scheme 1. Schematic diagram of the photogenerated electron-hole pairs separation and transport process of the photoanodes.

CoAl-LDHs/P-Fe_2O_3 photoanode was tested by chronoamperometry (Fig. 4d). After continuous exposure to AM 1.5 G illumination for 3 h, there is no obvious difference in the recorded photocurrent, indicating its excellent photoelectric stability.

Based on the above analysis, Scheme 1 is a schematic diagram of the photogenerated electron-hole pairs separation and transport process of the CoAl-LDHs/P-Fe_2O_3 composite photoanodes. Hematite suffers from severe surface charge recombination and sluggish water oxidation kinetics, which results in inferior PEC performance. Phosphorus anion as a donor dopant significantly increases the carrier density of hematite and reduces the resistance to charge transfer. Besides, the electronic structure change caused by P doping could remove part of the hematite surface trapping sites and reduce the surface charge capture. The CoAl-LDHs OECs can effectively improve the kinetics of water oxidation on the surface of the hematite photoanode, and promote the transport of holes into the electrolyte for water oxidation. Moreover, P anion doping and the loading of CoAl-LDHs cocatalysts can both inhibit surface charge recombination and facilitate surface charge separation. Through the conversion of Co cations to high valence states during the water oxidation process, the injection efficiency of photogenerated holes could be obviously enhanced. Owing to the successive modification of P doping and CoAl-LDHs OECs, the CoAl-LDHs/P-Fe_2O_3 photoanodes exhibit outstanding PEC water oxidation performance.

In summary, we designed a co-activation strategy to solve the charge recombination and sluggish surface reaction of α-Fe_2O_3 through P doping and the loading of CoAl-LDHs OECs. Among them, P anion doping significantly increases the carrier density of hematite and reduces the resistance of charge transfer. The CoAl-LDHs OECs not only accelerates the water oxidation kinetics of hematite but also effectively improves the injection efficiency of photogenerated holes through the conversion of cobalt ions. Besides, the P anion doping and the loading of the CoAl-LDHs OECs are both facilitated to the separation of the surface charge of the hematite, which is more effective for PEC water oxidation. As a result, the CoAl-LDHs/P-Fe_2O_3 photoanodes exhibits an outstanding photocurrent density of 1.56 mA/cm^2 at 1.23 V (*vs.* RHE), which is 2.6 times of pure α-Fe_2O_3. Besides, the onset potential is negatively shifted from 0.8 V to 0.7 V (*vs.* RHE) and the N_d of CoAl-LDHs/P-Fe_2O_3 photoanodes obtained from Mott-Schottky results is 1.84×10^{20} cm^{-3}. The ABPE achieves 0.20% at 1.0 V (*vs.* RHE), which is 3.84 times that of the bare α-Fe_2O_3 photoanodes, and the surface charge separation efficiency is increased to 68.8% at 1.23 V (*vs.* RHE). Our research demonstrates that co-activation of anion doping and cocatalysts is a favorable strategy to improve the PEC performance of hematite.

Declaration of competing interest

The authors report no declarations of interest.

Acknowledgments

This work was supported by the National Natural Science Foundation of China (No. 21575115); the Program for Chang Jiang Scholars and Innovative Research Team, Ministry of Education, China (No. IRT-16R61).

Appendix A. Supplementary data

Supplementary material related to this article can be found, in the online version, at doi:https://doi.org/10.1016/j.cclet.2021.01.003.

References

[1] D.K. Lee, K.S. Choi, Nat. Energy 3 (2018) 53–60.
[2] H.P. Ma, J.H. Yang, J.J. Tao, et al., Nano Energy 66 (2019) 104089.
[3] X. Ning, B. Lu, Z. Zhang, et al., Angew. Chem. Int. Ed. 58 (2019) 16800–16805.
[4] S. Corby, L. Francas, S. Selim, et al., J. Am. Chem. Soc. 140 (2018) 16168–16177.
[5] G. Ai, H. Li, S. Liu, R. Mo, J. Zhong, Adv. Funct. Mater. 25 (2015) 5706–5713.
[6] C.C. Li, Z.B. Luo, T. Wang, J.L. Gong, Adv. Mater. 30 (2018) 1707502.
[7] Y.J. Lin, S. Zhou, S.W. Sheehan, D.W. Wang, J. Am. Chem. Soc. 133 (2011) 2398–2401.
[8] S.R. Pendlebury, X. Wang, F. Le Formal, et al., J. Am. Chem. Soc. 136 (2014) 9854–9857.
[9] S. Kment, F. Riboni, S. Pausova, et al., Chem. Soc. Rev. 46 (2017) 3716–3769.
[10] F. Le Formal, S.R. Pendlebury, M. Cornuz, et al., J. Am. Chem. Soc. 136 (2014) 2564–2574.
[11] B.B. Zhang, L. Wang, Y.J. Zhang, Y. Ding, Y.P. Bi, Angew. Chem. Int. Ed. 57 (2018) 2248–2252.
[12] M. Wang, M. Wang, Y. Fu, S. Shen, Chin. Chem. Lett. 28 (2017) 2207–2211.
[13] S.S. Yi, B.R. Wulan, J.M. Yan, Q. Jiang, Adv. Funct. Mater. 29 (2019) 1801902.
[14] Y. Chao, P. Zhou, N. Li, et al., Adv. Mater. 31 (2019) 1807226.
[15] P. Peerakiatkhajohn, J.H. Yun, H.J. Chen, et al., Adv. Mater. 28 (2016) 6405–6410.
[16] L. Cai, Y.C. Du, X.J. Guan, S.H. Shen, Chin. Chem. Lett. 30 (2019) 2363–2367.
[17] J.W. Jang, C. Du, Y.F. Ye, et al., Nat. Commun. 6 (2015) 7447.
[18] C.X. Kronawitter, I. Zegkinoglou, S.H. Shen, et al., Energy Environ. Sci. 7 (2014) 3100–3121.
[19] R. Franking, L.S. Li, M.A. Lukowski, et al., Energy Environ. Sci. 6 (2013) 500–512.
[20] M.Y. Li, Y. Yang, Y.C. Ling, et al., Nano Lett. 17 (2017) 2490–2495.
[21] T.T. Jiao, C. Lu, D. Zhang, et al., Appl. Catal. B: Environ. 269 (2020) 118768.
[22] A. Bak, W. Choi, H. Park, Appl. Catal. B-Environ. 110 (2011) 207–215.
[23] P.L. Liao, M.C. Toroker, E.A. Carter, Nano Lett. 11 (2011) 1775–1781.
[24] H.J. Ahn, K.Y. Yoon, M.J. Kwak, J. Park, J.H. Jang, ACS Catal. 8 (2018) 11932–11939.
[25] Z.B. Luo, C.C. Li, S.S. Liu, T. Wang, J.L. Gong, Chem. Sci. 8 (2017) 91–100.
[26] Y. Zhang, S. Jiang, W. Song, et al., Energy Environ. Sci. 8 (2015) 1231–1236.
[27] A. Kubacka, M. Fernandez Garcia, G. Colon, Chem. Rev. 112 (2012) 1555–1614.
[28] D. Chen, Z.F. Liu, Z.G. Guo, M.N. Ruan, W.G. Yan, ChemSusChem 12 (2019) 3286–3295.
[29] W. Li, D. He, S.W. Sheehan, et al., Energy Environ. Sci. 9 (2016) 1794–1802.
[30] F. Li, J. Li, L.L. Gao, et al., J. Mater. Chem. A 6 (2018) 23478–23485.
[31] C.M. Li, Z.H. Chen, W.Y. Yuan, Q.H. Xu, C.M. Li, Nanoscale 11 (2019) 1111–1122.
[32] G. Wang, B.Y. Wang, C.H. Su, et al., J. Catal. 359 (2018) 287–295.
[33] R.F. Chong, B.Y. Wang, C.H. Su, et al., J. Mater. Chem. A 5 (2017) 8583–8590.
[34] S.L. Bai, H.M. Chu, X. Xiang, et al., Chem. Eng. J. 350 (2018) 148–156.
[35] C.L. Wang, X.F. Long, S. Wei, et al., ACS Appl. Mater. Interfaces 11 (2019) 29799–29806.
[36] G. Chen, R. Gao, Y. Zhao, et al., Adv. Mater. 30 (2018) 1704663.
[37] C. Li, A. Li, Z. Luo, et al., Angew. Chem. Int. Ed. 56 (2017) 4150–4155.
[38] A. Kay, I. Cesar, M. Gratzel, J. Am. Chem. Soc. 128 (2006) 15714–15721.
[39] J.F. Zhang, R. Garcia-Rodriguez, P. Cameron, S. Eslava, Energy Environ. Sci. 11 (2018) 2972–2984.
[40] T. Boningari, P.R. Ettireddy, A. Somogyvari, et al., J. Catal. 325 (2015) 145–155.
[41] Y. Du, Q. Wang, X. Liang, et al., J. Catal. 331 (2015) 154–161.
[42] Q. Rui, L. Wang, Y.J. Zhang, et al., J. Mater. Chem. A 6 (2018) 7021–7026.
[43] X. Ning, P. Du, Z. Han, J. Chen, X. Lu, Angew. Chem. Int. Ed. 59 (2020) 13014.
[44] R.Z. Ma, J.B. Liang, K. Takada, T. Sasaki, J. Am. Chem. Soc. 133 (2011) 613–620.
[45] Y.C. Zhang, S.Q. Jiang, W.J. Song, et al., Energy Environ. Sci. 8 (2015) 1231–1236.